Model-Based Active Thermal Management for Neutral-Point Clamped Power Converter with Adaptive Weight

S M Imrat Rahman[1]*, Ali Moghassemi[1], Laxman Timilsina[1], Payam Ramezani-Badr[1], Qilun Zhu[2], Robert Prucka[2], Gokhan Ozkan[1,3], Christopher S. Edrington[1],
Emails: {smimrar*;amoghas;ltimils;prameza;qilun;rprucka;gokhano;cedring}@clemson.edu
[1]*Holcombe Department of Electrical and Computer Engineering, Clemson University, Clemson 29634, SC, USA*
[2]*Department of Automotive Engineering, Clemson University, Greenville 29607, SC, USA*
[3]*Dominion Energy Innovation Center, Clemson University, North Charleston 29405, SC, USA*

2024 IEEE Transportation Electrification Conference and Expo (ITEC) | 979-8-3503-1766-4/24/$31.00 ©2024 IEEE | DOI: 10.1109/ITEC60657.2024.10599084

***Abstract*—Permanent Magnet Synchronous Machines (PMSM) are commonly used for Electric Vehicles (EV) to benefit from their higher torque and efficiency, better performance, and heat dissipation capability than an asynchronous machine. The reliability of the power converters of PMSM drives is crucial for EV operation and is mainly related to the junction temperature of semiconductor devices. During operation, semiconductors experience periodic heating and cooling processes, which causes thermal stress. This stress causes failures of the devices and increases maintenance costs. This paper uses the Finite Control Set Model Predictive Control (FCS-MPC) approach to provide active thermal management (ATM) for a motor drive system. Active thermal management is a method to reduce the thermal cycling of the semiconductor device in order to improve the reliability of the motor drive system. The proposed method uses the FCS-MPC method to predict the three-level Neutral-Point Clamped (3L-NPC) converter's electro-thermal characteristic to find its optimum state. The speed reference is converted to the reference current via Field-Oriented Control (FOC), and a Cauer-thermal network is used to predict the junction temperature of the semiconductors. The mission objectives vary during the EV operation; thus, adaptive weighting is applied to the objective function to control thermal cycling effectively. The preliminary results of the proposed method show that thermal cycling can be managed to improve reliability, and FCS-MPC is a powerful tool to provide multi-objective control for EV powertrains.**

***Index Terms*—Active Thermal Management (ATM), Finite Control Set Model Predictive Control (FCS-MPC), Neutral-Point Clamped (NPC) Converter.**

I. Introduction

Permanent Magnet Synchronous Machines (PMSM) have been used in different application areas, such as Electrical Vehicles (EVs), industrial drives, propulsion systems, and home appliances [1]. In recent years, most EV companies have focused on providing long-range, high-performance, reliable EVs and hybrid EVs (HEV) with better personal comfort levels, just like traditional Internal Combustion Engine (ICE) vehicles at a reasonable price [2]. The EVs' efficiency is crucial for a long-range drive, and many researchers consistently propose new approaches to improve the current EVs' range limits [3]. Designing compact power trains, reducing thermal losses, and improving power conversion efficiency are essential to reduce the cost of operation. Compared to ICE vehicles, HEVs require additional components such as batteries, electrical machines, and power converters, which might increase the size and weight of the vehicle. Power conversion efficiency should be lowered to optimize the vehicle's design by considering a higher range and lower cost.

An additional concern about EVs/HEVs is improving the reliability of electrical components. One of the main components of EVs and HEVs is power converters. Thanks to Silicon Carbide (SiC) technology, the power converters can provide better power quality and efficiency than the Si-based power converters due to higher switching capability and reduced losses. However, thermal stress is still the primary failure mechanism in semiconductor devices [4], [5]. The current flow on a semiconductor causes power losses on its substrates' layers, and these power losses cause heat generation. Due to each layer being built with different materials, the thermal coefficient of these materials also varies. When the semiconductors experience thermal cycling, the shear stresses between layers increase, and it might result in device failure. To improve the reliability and power losses of power converters, the junction temperature of the semiconductor can be controlled [6], [7].

For weight and size optimization, not only power converters are taken into account, but also their cooling systems are included. The cooling systems are relatively larger and heavier than semiconductors, especially when the power level is increased [5]. The cooling systems are primarily designed to reduce the junction temperature with constant speed and forced cooling (air or liquid coolant). This approach usually cannot prevent thermal cycling. However, in some applications, a variable-speed cooling system is used to reduce the thermal cycling on the device [8], [9]. This approach can reduce thermal cycling; however, control of the junction temperature is limited due to the higher thermal time constant than the electrical time constant. Thermal cycling primarily relates to ambient temperature, current flow through semiconductors, and switching frequency. Another approach to reducing thermal

DISTRIBUTION STATEMENT A. Approved for public release; distribution is unlimited. (OPSEC 5879) cycling is to control thermal-related parameters and losses on semiconductors [10], [11].

Active thermal management (ATM) controls the junction temperature of semiconductor devices to reduce temperature-related failures and improve system efficiency [10], [12]. In reference [12], optimum weighting factors are determined by running multiple simulations, and fixed weighting factors are used. The fixed weights might cause unnecessary switching when the operation point of the converter is changed. In addition, the proposed algorithm's performance is tested only for constant power operation; however, this might differ for EV applications. Controlling the thermal-related parameters offers a better dynamic response because the control action is applied during switching states [13].

A. State Of Contribution

This paper uses a three-phase, three-level inverter to drive a Permanent Magnet Synchronous Machine (PMSM) using the Finite Control Set Model Predictive Control (FCS-MPC) method by modifying gains in the objective function. The three-level inverter is chosen to reduce the current harmonics. A lumped-parameter thermal network is used to predict the junction temperature of SiC semiconductors. The control objectives are:

- Following the reference speed and torque of the PMSM.
- Reducing the thermal cycling of semiconductors by using adaptive weights.

The rest of the paper is organized as follows. The modeling and control design approach is described in Section II. The results of the simulations are given in Section III. The paper is concluded in Section IV.

II. Modeling and Control Design

First, a PMSM and a three-level, three-phase Neutral-Point-Clamped (3L-NPC) power converter are modeled to evaluate the performance of the proposed ATM strategy. The 3L-NPC converter consists of twelve Metal Oxide Semiconductor Field Effect Transistors (MOSFETs) and six clamping diodes, as shown in Fig. 1. The NPC power converter reduces the current harmonics and increases the available voltage vectors. For medium- to high-voltage applications, NPC power converters are commonly employed to reduce the blocked voltages and power losses of each semiconductor.

A. PMSM Model

The rate of current change for a PMSM, written in the synchronous reference frame, can be calculated using the expression (1) [14].

$$\begin{bmatrix} \frac{d}{dt} i_d \\ \frac{d}{dt} i_q \end{bmatrix} = \begin{bmatrix} \frac{1}{L_d} \\ \frac{1}{L_q} \end{bmatrix} \begin{bmatrix} v_d \\ v_q \end{bmatrix} + \begin{bmatrix} -\frac{R_s}{L_d} & \frac{p\omega L_q}{L_d} \\ -\frac{p\omega L_d}{L_q} & -\frac{R_s}{L_q} \end{bmatrix} \begin{bmatrix} i_d \\ i_q \end{bmatrix} + \begin{bmatrix} 0 \\ -\frac{\lambda p\omega}{L_q} \end{bmatrix} \tag{1}$$

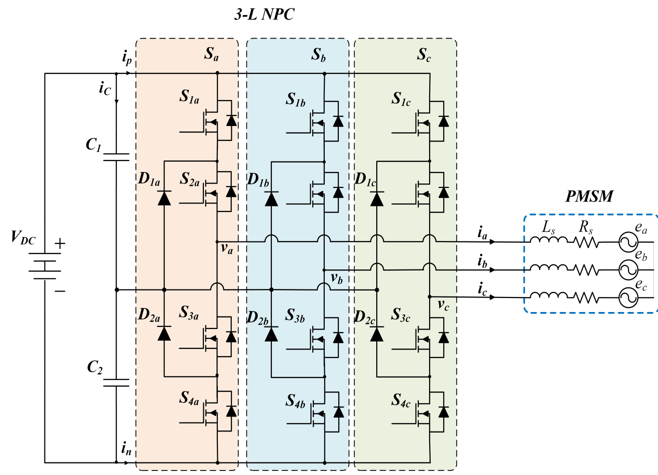

Fig. 1. Drive system with a three-level three-phase NPC power converter and PMSM

Here i_d,i_q,v_d,v_q,L_d and L_q are dq-axis currents, voltages and inductances, respectively, R_s is the resistance of stator windings, ω is angular rotor velocity, p is the number of poles and λ is the amplitude of the flux induced by permanent magnets. The forward Euler discretization method is used to discretize the expression (1). The forward Euler method is a first-order discretization method, which includes higher truncation errors than higher-order discretization methods. The truncation error for various discretization methods is investigated in [15]. As shown in expression (2), discrete-time predictive current can be obtained.

$$\begin{bmatrix} i_d(k+1) \\ i_q(k+1) \end{bmatrix} = \begin{bmatrix} \frac{1}{L_d} \\ \frac{1}{L_q} \end{bmatrix} \begin{bmatrix} v_d(k+1) \\ v_q(k+1) \end{bmatrix} + \begin{bmatrix} 1-\frac{R_s}{L_d} & \frac{p\omega L_q}{L_d} \\ -\frac{p\omega L_d}{L_q} & 1-\frac{R_s}{L_q} \end{bmatrix} \begin{bmatrix} i_d(k) \\ i_q(k) \end{bmatrix} + \begin{bmatrix} 0 \\ -\frac{\lambda p\omega}{L_q} \end{bmatrix} \tag{2}$$

In this paper, a 50 kW 8 pole IPMSM has been considered for analyzing the thermal performance of the NPC inverter. The specification of the motor is presented in Table I.

TABLE I
PMSM Parameters

Parameter	Value	Unit
Rated power	50	kW
Pole pairs	4	-
Base speed	3000	rpm
Base torque	159.17	Nm
Rated current	96	A
Winding resistance per phase	0.0079	Ω
Inductance per phase	0.87	mH
Permanent magnet flux linkage	0.104	V.s
Inertia	0.82	kg*m^2

B. Converter Model

To develop a 3L-NPC model, all the possible switching states should be considered. The NPC converter has three legs, each with three switching states; therefore, a total of twenty-seven (3^3) switching states can be obtained for it. The switching states for each leg can be three different values as expressed in (3). Here, x indicates the three phases (a, b, c).

$$S_x = \begin{Bmatrix} 1(P) & if & S_{1x} \; and \; S_{2x} \; are \; on \\ 0 & if & S_{2x} \; and \; S_{3x} \; are \; on \\ -1(N) & if & S_{3x} \; and \; S_{4x} \; are \; on \end{Bmatrix} \tag{3}$$

As can be seen from (2), all the variables except $v_d(k)$ and $v_q(k)$ (converter voltages) are either known or measured. The converter voltages can be predicted using (4).

$$\begin{bmatrix} v_d(k+1) \\ v_q(k+1) \end{bmatrix} = \frac{2V_{\text{DC}}}{6} \begin{bmatrix} \cos\theta & \sin\theta \\ -\sin\theta & \cos\theta \end{bmatrix} \times \begin{bmatrix} 1 & -\frac{1}{2} & -\frac{1}{2} \\ 0 & \frac{\sqrt{3}}{2} & -\frac{\sqrt{3}}{2} \end{bmatrix} \begin{bmatrix} S_a \\ S_b \\ S_c \end{bmatrix} \tag{4}$$

C. Loss Model

The main losses for semiconductors are conduction and switching losses. The switching losses are dependent on current, voltage, and junction temperature. Therefore, (5) and (6) are derived from reference [16] for calculating the switching losses. Conduction losses for a SiC MOSFET and diode can be calculated using (7) and (8).

$$E_{\text{sw,MO}} = (E_{\text{on}} + E_{\text{off}}) \left(\frac{i_D}{i_{\text{ref}}}\right)^{K_{i,\text{MO}}} \times \left(\frac{v_{\text{dc}}}{v_{\text{ref}}}\right)^{K_{v,\text{MO}}} \times \left(1 + c_{T,\text{sw}} \left(T_{j,\text{MO}} - T_{j,\text{MO,ref}}\right)\right) \tag{5}$$

$$E_{\text{sw,d}} = E_{\text{rr}} \left(\frac{i_f}{i_{d,\text{ref}}}\right)^{K_{i,d}} \times \left(\frac{v_f}{v_{d,\text{ref}}}\right)^{K_{v,d}} \times \left(1 + c_{T,\text{rr}} \left(T_{j,d} - T_{j,d,\text{ref}}\right)\right) \tag{6}$$

$$P_{\text{cond,ig}} = R_{\text{DS(on)}} \cdot i_D^2 \tag{7}$$

$$P_{\text{cond,d}} = V_{\text{SD}} \cdot i_f \tag{8}$$

Here E_{on} and E_{off} are the turn-on and turn-off switching energy, E_{rr} is the diode recovery energy, i_{ref},v_{ref},$T_{j,MO,ref}$ and $T_{j,d,ref}$ are the reference operation: current, voltage, and MOSFET and diode junction temperature from the module's datasheet. K_v,K_i,$c_{T,sw}$ and $c_{T,rr}$ are empirically obtained constants, and i_D and i_f are MOSFET drain and forward current, $R_{DS(on)}$ is MOSFET on-state resistance, V_{SD} is the forward voltage of the anti-parallel diode.

D. Thermal Model

The junction temperature of the semiconductor devices can be estimated by physical contact and optical techniques, temperature-sensitive electrical parameters (TSEPs), and thermal network-based models [17], [18]. Among these methods, the thermal network-based model has been favored for this study due to its suitability for online junction temperature measurement and its independence from additional measuring circuits. These thermal networks employ thermal resistance and capacitance to represent the heat conduction path within semiconductor materials. Cauer and Foster networks are two common forms of thermal circuits extensively utilized for thermal modeling. In this study, a Cauer-type thermal network is used to predict the junction temperature of the semiconductors [13]. The model parameters (thermal capacitance and resistance) are estimated using SaberRD software. A third-order (n=3) Cauer-type thermal network with a lumped parameter representation of thermal resistance (R_{th}) and capacitance (C_{th}), representing each layer of the semiconductor device has been used in this study. The equivalent thermal impedance (Z_{th}) and junction temperature (T_j) of a single switch are expressed using (9) and (10), where P_L, and T_C are power losses and ambient temperature, respectively.

$$Z_{th}\left(t\right) = \sum_{i=1}^{n} \left(1 - e^{-\frac{t}{R_{th,i} C_{th,i}}}\right) \tag{9}$$

$$T_j\left(t\right) = P_L\left(t\right) Z_{th}\left(t\right) + T_c(t) \tag{10}$$

E. Cost Function

A multiple-objective cost function is used to reduce current ripples and thermal cycling. A generalized multi-objective function for the FCS-MPC is given as:

$$J = \lambda_E \left[(i_d^*(k+1) - i_d(k+1))^2 + (i_q^*(k+1) - i_q(k+1))^2\right] + \lambda_{TH} \left|T_j^*(k+1) - T_j(k+1)\right| \tag{11}$$

The first part of the cost function is used to control the electrical performance of the power converter. The predicted currents, $i_d(k+1)$ and $i_q(k+1)$, are compared to their references. The second part of the cost function is derived from controlling the junction temperature of the power module. $T_j(k{+}1)$ is estimated using (10), and the error with its reference is calculated. The weight factors (λ_E and λ_{TH}) are firstly tuned by using trial-and-error method, and the relation between λ_E and λ_{TH} is expressed using (12)

$$\lambda_E + \lambda_{TH} = 1 \tag{12}$$

The safe operating range for λ_E is determined to be between 0.4 to 1. An algebraic optimization, which compares all the possible solutions (19 different solutions for electrical cost function and 27 possible solutions for thermal cost function), is used to find the optimum solution for thermal and electrical performance.

F. Control Framework

The conventional FCS-MPC introduces variable switching frequency; however, it can be fixed by including an additional penalty factor on the objective function. This study uses a variable switching frequency to manipulate the switching losses. The cost function determines the switching states, and an adaptive weight factor scheme is implemented to improve the performance of the control algorithm. The control algorithm and physical system, as shown in Fig. 2, are designed in MATLAB/Simulink. Field-oriented Control (FOC) is used to generate the reference current signals $i_d^*(k+1)$ and $i_q^*(k+1)$ for the FCS-MPC algorithm and the weight factor related to the electrical performance of the PMSM, λ_E, is controlled with a PI controller. A single prediction and control horizon is used for this study to reduce the computational burden. The predicted currents and junction temperatures are calculated using (2) and (10) for available voltage vectors for every 50 µs. Finally, the switching state that provides minimum error is applied to the power converter. When the difference between the junction temperature and its reference increases, the thermal weight value is increased by a PI controller, which means the control algorithm decision will shift more to thermal performance.

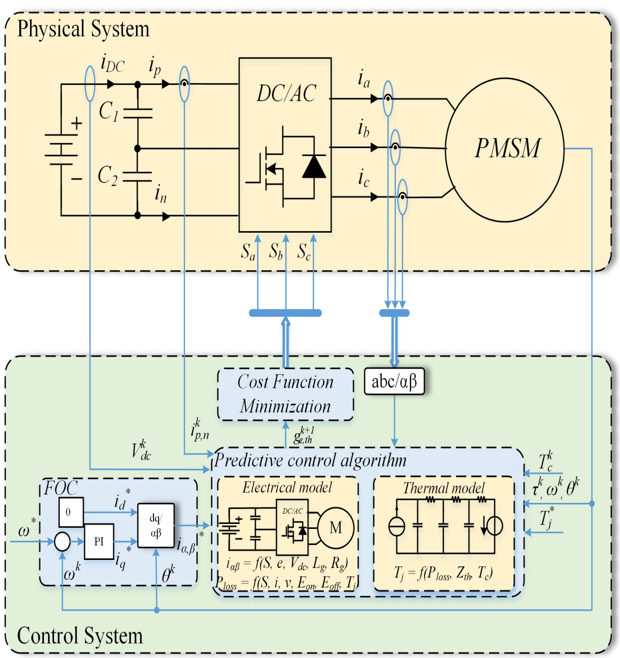

Fig. 2. Proposed drive system and control framework

III. Simulation Results

The simulation results for a 3L-NPC power converter with FCS-MPC are presented in this section. Three cases have been considered to evaluate the performance of the proposed ATM strategy, and the junction temperature of the hottest MOSFET switch is presented for comparison. A desktop computer with an Intel I7-8700 3.2 GHz CPU and 16 Gb DDR4-2666 MHz RAM is used for simulation. In the physical system (Fig. 2), the sampling time is chosen as 10 µs, and the control system sampling time is chosen as the same as the prediction horizon, which is 50 µs. The computational time for 15 seconds full system simulation is 1002.36 seconds and the computational time for a single prediction horizon of the control system has an average value of 291.9 µs.

A. Case A

In the first case, conventional FCS-MPC, where λ_E=1, is used to create a baseline. Figures 3a and 3b show the machine currents and generated reference currents, respectively. Moreover, it can be observed from Fig. 3c that the control system can track the reference speed accurately. However, as shown in Fig. 3d, increasing the load torque at t = 7s causes 39°C thermal cycling. Similarly, when the load torque is reduced at t = 10s, junction temperature deviation reaches 53°C. These large thermal swings pose a risk to the reliability of MOSFET devices and could potentially lead to their failure.

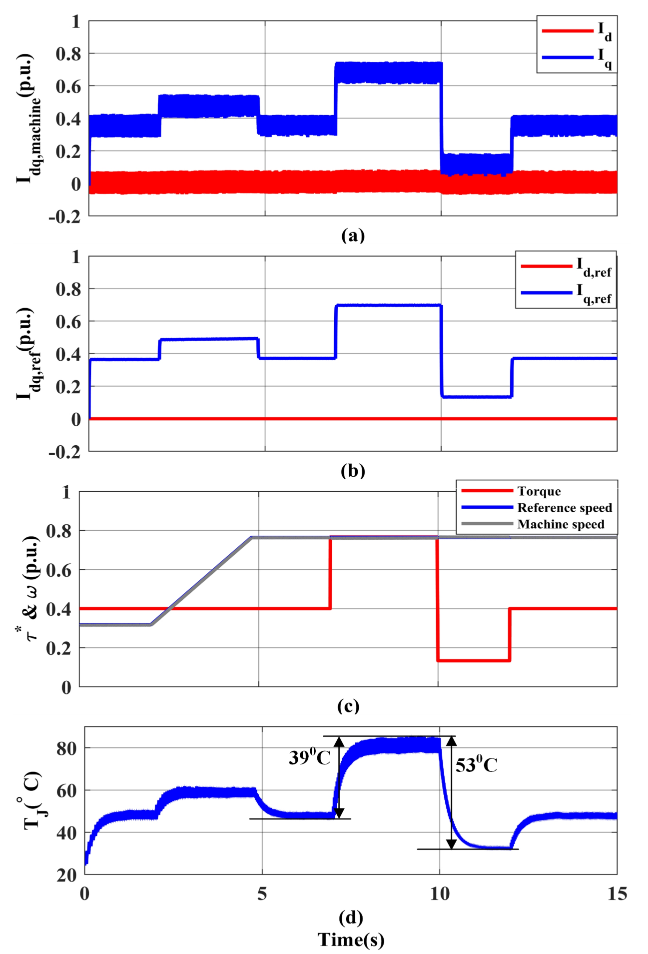

Fig. 3. Simulation results with conventional FCS-MPC and no ATM (a) Machine currents (b) Reference currents (c) Speed tracking performance (d) Thermal performance

B. *Case B*

In the second case, the performance of the ATM strategy with a constant weight factor (λ_E=0.5) is presented. As seen from Fig. 4d, the total junction temperature deviation is reduced by 12°C and 14°C compared to the first case. However, current ripples are increased due to less switching action, which can be seen in Fig. 4a and Fig. 4b. Moreover, the speed tracking performance deteriorates slightly compared to *Case A*.

C. *Case C*

In the last case, an adaptive weight scheme is applied, and a further reduction in MOSFET thermal cycling is observed, as shown in Fig. 5d. The adaptive weight scheme updates the thermal weighting factor depending on the deviation of the estimated junction temperature compared to the reference junction temperature, as shown in Fig. 5e. In this case, the reference junction temperature was set to 65°C. Whenever the estimated junction temperature crossed this threshold value, the adaptive weight scheme changed the values of ω_e and ω_{th}. In addition, the current ripples are reduced compared to

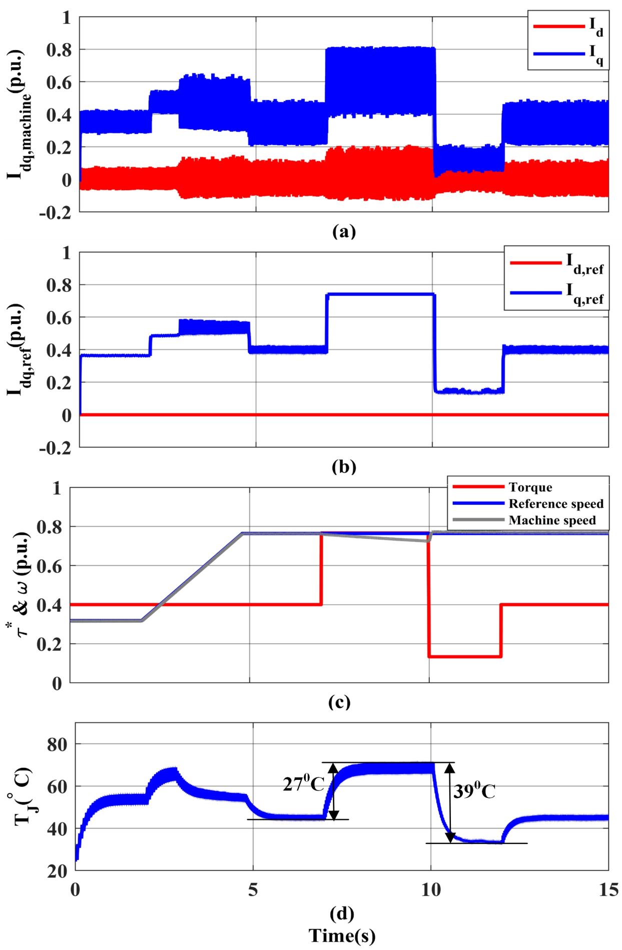

Fig. 4. Simualtion results with ATM and constant weight (λ_E=0.5) (a) Machine currents (b) Reference currents (c) Speed tracking performance (d) Thermal performance

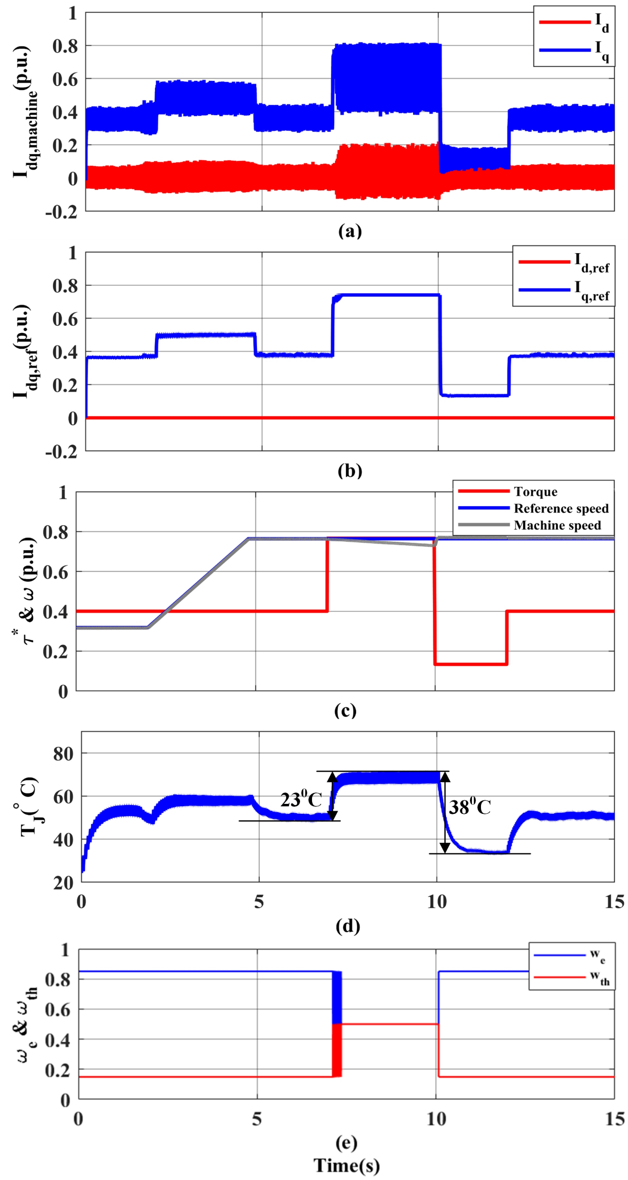

Fig. 5. Simualtion results with ATM and adaptive weight (a) Machine currents (b) Reference currents (c) Speed tracking performance (d) Thermal performance (e) Electrical and thermal weight

the second case, as shown in Fig. 5a and Fig. 5b. Moreover, the speed tracking performance deteriorates slightly during high-loading conditions compared to *Case A*.

A comparison of thermal cycles for the three different cases is presented in Table II. It can be seen that ATM with an adaptive weight scheme achieved the maximum reduction in thermal cycles.

IV. Conclusion

An active thermal management scheme with adaptive weight for PMSM drives with 3L-NPC is presented in this work. The results show that the performance of the control algorithm can be improved by using adaptive weight on the objective

TABLE II
COMPARISON OF THERMAL PERFORMANCE

Case	Largest thermal cycle	2nd largest thermal cycle
A	53°C	39°C
B	39°C	27°C
C	38°C	23°C

function. The constant weight might be efficient for constant loading conditions such as cooling systems and fan applications; however, adaptive weights provide better performance if the converter loading is unknown. The drawback of the proposed algorithm is increased current ripples due to reduced average switching frequency; therefore, current harmonics should be taken into account depending on the application.

The real-time implementation of the proposed method is left for future work. For real-time implementation, a simplified MPC and/or sector distribution method might be necessary to reduce the computational time.

ACKNOWLEDGMENT

This work was supported by the Automotive Research Center (ARC), a US Army Center of Excellence for modeling and simulation of ground vehicles, under Cooperative Agreement W56HZV-19-2-0001 with the US Army DEVCOM Ground Vehicle Systems Center (GVSC). This document is approved for Distribution A (Approved for public release; distribution unlimited), and Operations Security (OPSEC) review number is OPSEC5879.

The authors would like to acknowledge the Warren H. Owen Distinguished Professorship Endowment for its support of the research effort.

REFERENCES

[1] J. F. Gieras, *Permanent Magnet Motor Technology: Design and Applications*, 3rd ed. Boca Raton, FL, USA: CRC Press, 2010.

[2] Q. Zhu, et al., "Fast Engine Torque Variation Compensation for HEVs Using Permanent Magnet Synchronous Motor and Explicit MPC," *SAE Technical Paper*, No. 2021-01-0718. 2021, doi: 10.4271/2021-01-0718.

[3] C. Zhao, et al., "Research on Key Factors for Range and Energy Consumption of Electric Vehicles," *SAE Technical Paper*, No. 2019-01-0723, 2019, doi: 10.4271/2019-01-0723.

[4] H. Wang, M. Liserre and F. Blaabjerg, "Toward Reliable Power Electronics: Challenges, Design Tools, and Opportunities," *IEEE Industrial Electronics Magazine*, vol. 7, no. 2, pp. 17-26, 2013, doi: 10.1109/MIE.2013.2252958.

[5] J. Falck, G. Buticchi and M. Liserre, "Thermal Stress Based Model Predictive Control of Electric Drives," *IEEE Transactions on Industry Applications*, vol. 54, no. 2, pp. 1513-1522, 2018, doi: 10.1109/TIA.2017.2772198.

[6] G. Ozkan, et al. "Electro-Thermal Control on Power Electronic Converters: A Finite Control Set Model Predictive Control Approach." *SAE International Journal of Advances and Current Practices in Mobility*, vol. 4, no. 1, pp. 151-156, 2022, doi: 10.4271/2021-01-0200.

[7] M. Andresen, K. Ma, G. Buticchi, J. Falck, F. Blaabjerg and M. Liserre, "Junction Temperature Control for More Reliable Power Electronics," *IEEE Transactions on Power Electronics*, vol. 33, no. 1, pp. 765-776, Jan. 2018, doi: 10.1109/TPEL.2017.2665697.

[8] X. Wang, Y. Wang and A. Castellazzi, "Reduced active and passive thermal cycling degradation by dynamic active cooling of power modules," *2015 IEEE 27th International Symposium on Power Semiconductor Devices & IC's (ISPSD)*, Hong Kong, China, 2015, pp. 309-312, doi: 10.1109/ISPSD.2015.7123451.

[9] S. M. I. Rahman et al., "Impact of Active Cooling on the Thermal Management of 3-Level NPC Converter for Hybrid Electric Vehicle Application," *SAE Technical Paper*, No. 2023-01-1684, 2023, doi: 10.4271/2023-01-1684.

[10] G. Ozkan, et al. "Real-time thermal management for two-level active rectifier with finite control set model predictive control." *International Journal of Electrical Power & Energy Systems*, vol. 131, 2021,: 107057, doi: 10.1016/j.ijepes.2021.107057.

[11] A. Moghassemi, S. M. I. Rahman, G. Ozkan, C. S. Edrington, Z. Zhang and P. K. Chamarthi, "Power Converters Coolant: Past, Present, Future, and a Path Toward Active Thermal Control in Electrified Ship Power Systems," *IEEE Access*, vol. 11, pp. 91620-91659, 2023, doi: 10.1109/ACCESS.2023.3308523.

[12] M. Novak, T. Dragicevic and F. Blaabjerg, "Finite Set MPC Algorithm for Achieving Thermal Redistribution in a Neutral-Point-Clamped Converter," *IECON 2018 - 44th Annual Conference of the IEEE Industrial Electronics Society*, Washington, DC, USA, 2018, pp. 5290-5296, doi: 10.1109/IECON.2018.8591148.

[13] J. Falck, M. Andresen and M. Liserre, "Thermal-based finite control set model predictive control for IGBT power electronic converters," *2016 IEEE Energy Conversion Congress and Exposition (ECCE)*, Milwaukee, WI, USA, 2016, pp. 1-7, doi: 10.1109/ECCE.2016.7855513.

[14] R. H. Park, "Two-reaction theory of synchronous machines generalized method of analysis-part I," *Transactions of the American Institute of Electrical Engineers*, vol. 48, no. 3, pp. 716-727, July 1929, doi: 10.1109/T-AIEE.1929.5055275.

[15] A. M. A. Almaktoof, *Multi-level inverters using finite set-model predictive current control for renewable energy systems applications*, PhD Dissertation, Electrical Engineering Department, Cape Peninsula University of Technology, Cape Town, South Africa, 2015.

[16] G. Lakkas, "MOSFET power losses and how they affect power-supply efficiency," *Analog Applications Journal*, vol. 10, no. 2016:22-26, 2016.

[17] M. H. M. Sathik, J. Pou, S. Prasanth, V. Muthu, R. Simanjorang and A. K. Gupta, "Comparison of IGBT junction temperature measurement and estimation methods-a review," *2017 Asian Conference on Energy, Power and Transportation Electrification (ACEPT)*, Singapore, 2017, pp. 1-8, doi: 10.1109/ACEPT.2017.8168600.

[18] Z. Zhang et al., "Online Junction Temperature Monitoring Using Intelligent Gate Drive for SiC Power Devices," *IEEE Transactions on Power Electronics*, vol. 34, no. 8, pp. 7922-7932, Aug. 2019, doi: 10.1109/TPEL.2018.2879511.